Measurement 170 (2021) 108679

Contents lists available at ScienceDirect

Measurement

journal homepage: www.elsevier.com/locate/measurement

A hybrid prognostic strategy with unscented particle filter and optimized multiple kernel relevance vector machine for lithium-ion battery

Xiaofei Sun [a], Kai Zhong [a], Min Han [b,*]

[a] Faculty of Electronic Information and Electrical Engineering, Dalian University of Technology, Dalian 116024, China
[b] Key Laboratory of Intelligent Control and Optimization for Industrial Equipment of Ministry of Education, Dalian University of Technology, Dalian 116024, China

ARTICLE INFO

Keywords:
State of health estimation
Remaining useful life prediction
Lithium-ion battery capacity estimation
Unscented particle filter
Optimized multiple kernel relevance vector machine

ABSTRACT

To make up the deficiencies of single methods in lithium-ion battery state of health (SOH) and remaining useful life (RUL) estimation, this paper presents a novel hybrid method using unscented particle filter (UPF) with optimized multiple kernel relevance vector machine (OMKRVM). Firstly, the errors between the initial estimation by UPF and the actual capacity are obtained. After that, the residuals are reconstructed by complementary ensemble empirical mode decomposition (CEEMD) to reduce interference. In addition, OMKRVM is adopted to provide multiple predictive abilities, and kernel parameters and weights of OMKRVM are yielded by the grid search. Finally, the initial estimation is corrected by the predicted residuals using OMKRVM to further improve prediction performance. The new method (UPF-OMKRVM) is compared with existing methods in predicting the degradation process of lithium-ion battery. The experimental results show that the UPF-OMKRVM has high prediction accuracy in lithium-ion battery SOH and RUL estimation.

1. Introduction

As the operating time of complex industrial systems increases, wear and aging is inevitable, and damaged equipment will reduce system reliability and even cause major accidents. The prognostics and health management (PHM) can implement early fault diagnosis and prognostics in the process of system degradation based on existing and historical data and models, so that we can know the trend of fault occurrence [1–3]. When the performance status of the equipment or the end of life (EOL) is estimated, maintenance management can be performed ahead of time to prevent major dangerous accidents, decrease the cost of maintenance operations, and significantly improve the safety and reliability of industrial systems [4,5]. Therefore, the role of PHM in complex industrial operation and maintenance is becoming more and more important, and it has also become a research hotspot today [6,7]. Lithium-ion battery is commonly used in various fields due to its safety, stability, long-life and low-polluting. In the PHM methodology of lithium-ion battery, state of health (SOH) estimation and remaining useful life (RUL) prediction are the research core [8], which can generally be classified into two categories: model-based methods and data-driven based methods [9].

Model-based methods rely on pre-established models to prognosticate the failure process of the system. Model-based methods are methods that use physical or first-principles to accurately describe the system. The identification and updating of model parameters usually require specially designed experimental and statistical methods, respectively. Therefore, when we have sufficient knowledge of mathematical and physical mechanisms, the methods tend to perform better than others. The Kalman filter (KF) method is relatively simple to iteratively calculate, and directly update the state to predict the output, so as to obtain prediction output. Lim et al. proposed a new state-space-based approach which using switched Kalman filter (SKF) for model estimation and RUL prognostic [10]. Compared with KF, particle filter (PF) has better performance, has the ability of probability expression, and is suitable for nonlinear non-Gaussian systems. Meanwhile, other excellent algorithms are proposed based on the standard PF. Zhang et al. proposed an unscented particle filter (UPF) based on linearly optimized combined resampling. The linearly combined resampling method was used to make up for the shortcomings of the lack of particle diversity [11]. Liu et al. proposed a battery SOH online prediction approach based on UPF. A model between health indicators (HI) is established to achieve state space model observation [12]. Although the model-based prediction methods has relatively high prediction accuracy, most of the above methods are carried out without error-correction, so the prediction

* Corresponding author.
E-mail address: minhan@dlut.edu.cn (M. Han).

https://doi.org/10.1016/j.measurement.2020.108679
Received 2 July 2020; Received in revised form 15 October 2020; Accepted 26 October 2020
Available online 2 November 2020

accuracy needs to be further improved.

The data-driven prediction methods mainly analyze the observed data to determine the SOH of the system within a certain time. Through various data processing and analysis methods (mostly statistical knowledge and machine learning knowledge) to mine the health status or degradation feature information implicit in the target system data, we can obtain the degradation tendency of system failure and the time to reach the failure threshold. Especially lack of comprehension of the system under consideration, data-driven forecasting is the preferred method [13]. Zhang used the least squares support vector machine method for fault prognostics and used particle swarm optimization (PSO) to optimize support vector machines and kernel parameters [14]. Relevance vector machine (RVM) algorithm has simple hyper-parameters, the characteristics of automatic parameter setting and arbitrary use of kernel parameters, and can provide probabilistic prediction results. Because of these advantages, RVM is widely applied to the field of fault prognostics. Wang et al. established a multi-step RVM offline model and updated the time-varying parameters with the expectation maximization algorithm. He also expressed the uncertainty as the variance of the parameter's Gaussian distribution, and quantified it as a time-varying variable [15]. Zhang et al. introduced a method combined Empirical mode decomposition (EMD) with multiple kernel relevance vector machine (MKRVM) to estimate RUL of NASA battery data. The measured data was reconstructed by EMD to obtain the noise-free data, and the model is established by using MKRVM [16]. Because the data-driven methods are based only on datasets without system physics knowledge, which may lead to the poor prediction results. Although some metaheuristics are used to select the sparse weights of the MKRVM kernel function, the optimization algorithm is prone to fall into the local optimum and sometimes too slow, resulting in poor prediction performance.

However, we found that single method is difficult to achieve accurate prediction, and for complex technical systems with many parameters changing over time. Because the parameters are constantly changing during the entire system degradation process, no matter which method is used, it may produce accumulating errors and causing significant deviations, the model-based approaches rely on physical models for state prediction, while the data-driven approach does not consider physical processes. To ease the problem, the hybrid approach which combining the strong points of both model-based and data-driven approach is considered to be more applicable when dealing with new environments. Song et al. proposed a hybrid approach which iterative updated parameters of prediction model. He applied the KF to optimize estimations of physical model and used the optimized estimations as the training data, so that the RVM model is re-trained to make next iterative prediction [17]. Zheng et al. used the relevance vector regression (RVR) model as a non-linear prediction model to prognosticate the future residual of the UKF, and then the UKF is applied to recursively estimate the parameters of model to predict the RUL combined the future residual [18]. However, this method adopted single kernel function and only had one single predictive ability, so the prediction of residuals may be unsatisfactory. Yang et al. proposed a hybrid prediction algorithm of PF and RVM to predict the noise interference in PF prediction algorithm through RVM. Due to the particle degeneration, noise interference and the prediction errors without reducing the noise interference, the forecasting results are not satisfactory [19].

Therefore, considering the limitations in the above literatures, we propose UPF-OMKRVM method to combine the advantages of UPF and OMKRVM, and overcome their limitations. First, the UPF method has better effect in filtering accuracy and reduces the affection of the particle degeneration, which is used to estimate the system state, thereby tracking the degradation process. Meanwhile, we can obtain the original error data between estimated value and true value. Then, the obtained error data are first subjected to CEEMD method to reduce noise [20]. To accurately predict errors evolutionary trend, we adopt multiple kernel RVM rather than single kernel. In addition, the optimal parameters of OMKRVM are obtained by grid search algorithm. Finally, the predicted errors are used to correct the initial estimation result. Through the error-correction in time, the accuracy of forecast can be improved significantly. Contrast experiments are performed in two lithium-ion battery degradation processes and verify the reliability and robustness of the proposed hybrid method.

The remainder of this paper is organized as follows: Section 2 introduces the principles of some basic algorithms in UPF-OMKRVM method. Section 3 provides model building of hybrid methods and the detailed implementation process. Section 4 introduces the lithium-ion battery set, the simulation experiments, results, and discussion. Section 5 is the conclusion.

2. Preliminaries

In this section, to better understand the UPF-OMKRVM proposed in this paper, the UPF, RVM and CEEMD algorithms are briefly reviewed.

2.1. Unscented particle filter

PF algorithm is one of the statistical filtering algorithm and uses particles to represent posterior probability distribution of states to solve the Bayesian estimation problem. The UPF algorithm combines the advantages of UKF and PF, and it consists of two parts: (1) Gain the particle recommendation distribution by UKF and obtain the posterior probability according to the latest observation [21]. (2) Use the standard PF method to give an estimate of the state variables and update the response covariance matrix.

Many industrial problems can be described with a dynamic system model, and the state-space model is described as follows,

$$\begin{cases} x_k = f(x_{k-1}, \omega_k) \\ y_k = h(x_k, \nu_k) \end{cases} \tag{1}$$

$k = 1, 2\cdots$ is a discrete time series, x_k is state characterization signal, f denote state transition function, ω_k is state disturbance or system noise, y_k is observation vector obtained at time k, h is observation function of state, ν_k is observed noise vector. The basic steps of the UPF is briefly described as follows.

Step 1: Initialization. Set $k = 0$, $\{x_0^i\}_{i=1}^N$ are sample particles.

$$\begin{aligned} \bar{x}_0 &= E[x_0] \\ P_0 &= E\left[\left(x_0 - \bar{x}_0\right)\left(x_0 - \bar{x}_0\right)^T\right] \\ x_0^a &== \left[\bar{x}_0 \ 00\right]^T \\ P_0^a &= E\left[\left(x_0^a - \bar{x}_0^a\right)\left(x_0^a - \bar{x}_0^a\right)^T\right] = diag(P_0, Q_0, R_0) \end{aligned} \tag{2}$$

Step 2: Update the particles by UKF method, compute and choose the particles sigma point set.

Sigma points and weights calculation:

$$\begin{aligned} x_k^a &= \left[x_k^T; \omega_k^T; v_k^T\right] \\ P_k^a &= E\left[\left(x_k^a - x_k^a\right)\left(x_k^a - x_k^a\right)^T\right] = diag(P_k, Q_k, R_k) \end{aligned} \tag{3}$$

Draw particles:

$$x_{k-1}^a = \left[\bar{x}_{k-1}^a \;\; \bar{x}_{k-1}^a + \sqrt{(n_a+\lambda)P_{k-1}^a} \;\; \bar{x}_{k-1}^a - \sqrt{(n_a+\lambda)P_{k-1}^a}\right]$$
$$n_a = n_x + n_\omega + n_\nu$$
$$\lambda = \alpha^2(n+k) - n$$
$$x_{k-1}^a = \left[x_{k-1}^x \;\; x_{k-1}^\omega \;\; x_{k-1}^\nu\right]^T \tag{4}$$
$$W_0^{(m)} = \frac{\lambda}{n_x+\lambda}$$
$$W_0^{(c)} = \frac{\lambda}{n_x+\lambda} + \left(1-\alpha^2+\beta\right)$$
$$W_j^{(m)} = W_j^{(c)} = \frac{1}{2(n_x+k)}, j = 1,2,\cdots 2n_x$$

n_x is the dimension of the state vector, n_ω, n_ν are the number of process and measurement noise.

Step 3: Time update:

$$x_{k|k-1}^x = f\left(x_{k-1}^x, x_{k-1}^\omega\right)$$
$$\bar{x}_{k|k-1} = \sum_{j=0}^{2n_a} W_j^{(m)} x_{k|k-1}^x$$
$$P_{k|k-1} = \sum_{j=0}^{2n_a} W_j^{(c)}\left[x_{j,k|k-1}^x - \bar{x}_{k|k-1}\right]\left[x_{j,k|k-1}^x - \bar{x}_{k|k-1}\right]^T \tag{5}$$
$$y_{k|k-1} = h\left(x_{k|k-1}^x, x_{k|k-1}^n\right)$$
$$\bar{y}_{k|k-1} = \sum_{j=0}^{2n_a} W_j^{(m)} y_{j,k|k-1}$$

Step 4: Measurement update:

$$P_{y_{k|k-1}y_{k|k-1}} = \sum_{j=0}^{2n_a} W_j^{(c)}\left[y_{j,k|k-1} - \bar{y}_{k|k-1}\right]\left[y_{j,k|k-1} - \bar{y}_{k|k-1}\right]^T$$
$$P_{x_{k|k-1}y_{k|k-1}} = \sum_{j=0}^{2n_a} W_j^{(c)}\left[x_{j,k|k-1} - \bar{x}_{k|k-1}\right]\left[y_{j,k|k-1} - \bar{y}_{k|k-1}\right]^T \tag{6}$$
$$K_k = P_{x_{k|k-1}y_{k|k-1}} P_{y_{k|k-1}y_{k|k-1}}^{-1}$$
$$\bar{x}_k = \bar{x}_{k|k-1} + K_k\left(y_k - \bar{y}_{k|k-1}\right)$$
$$\widehat{P}_k = P_{k|k-1} - K_k P_{y_{k|k-1}y_{k|k-1}} K_k^T$$

Step 5: Sampling:

$$\widehat{x}_k^i \sim q\left(x_k^i \middle| x_{k-1}^i, y_k\right) = N\left(\bar{x}_k^i, \widehat{P}_k^i\right) \tag{7}$$

Step 6: Weights calculation

$$\omega_k^i = \frac{p\left(x_{0:k}^i \middle| y_{1:k}\right)}{q\left(x_{0:k}^i \middle| y_{1:k}\right)} = \omega_{k-1}^i \frac{p\left(y_k \middle| x_k^i\right) p\left(x_k^i \middle| x_{k-1}^i\right)}{q\left(x_k^i \middle| x_{k-1}^i, y_k\right)} \tag{8}$$

Step 7: Normalize the weights and resampling:

$$\tilde{\omega}_k^i = \frac{\omega_k^i}{\sum_{j=1}^N \omega_k^j} \tag{9}$$

$$\tilde{\omega}_k^i = \frac{1}{N} \tag{10}$$

Step 9: State estimation:

$$\tilde{x}_k^i = \sum_{i=1}^N \tilde{\omega}_k^i x_k^i$$
$$P_k^i = \sum_{i=1}^N \tilde{\omega}_k^i \left[x_k^i - \tilde{x}_k^i\right]\left[x_k^i - \tilde{x}_k^i\right]^T \tag{11}$$

2.2. Relevance vector machine

RVM includes relevance vector regression and relevance vector classification. RUL prediction is essentially a relevance vector regression problem [22].

For a given data set $\{x_i, t_i\}_{i=1}^N$, $x_i \in R^d$, N is the quantity of samples. The non-linear model is:

$$t = y(x) + \varepsilon = \Phi\omega + \varepsilon \tag{12}$$

$y(\cdot)$ is non-linear function, $\omega = [\omega_0, \cdots, \omega_N]$ is the RVR weight, $\Phi = [\varphi_1, \varphi_2, \cdots \varphi_N,]$ is the kernel function matrix and $\varphi(x_i) = [1, K(x_i, x_1), \cdots, K(x_i, x_N)]$. $K(x_i, x_j)$ is kernel function, ε is an independent Gaussian noise.

According to Bayesian inference, the possibility estimate of the data set is:

$$p\left(t\middle|\omega,\sigma^2\right) = \left(2\pi\sigma^2\right)^{-N/2} exp\left\{-\|t-\Phi\omega\|^2 \middle/ 2\sigma^2\right\} \tag{13}$$

If the maximum likelihood estimation is performed directly on the weights, serious overfitting phenomenons may occur. Therefore, a form of weight hyperparameters is given.

$$p(\omega/\alpha) = \prod_0^N N\left(\omega_i\middle|0,\alpha_i^{-1}\right) = \prod_0^N \frac{\alpha_i}{\sqrt{2\pi}} \exp\left(\frac{\omega_i^2\alpha_i}{2}\right) \tag{14}$$

where $\alpha = \{\alpha_0, \alpha_1, \cdots, \alpha_N\}$, and the N + 1 hyperparameters correspond to ω.

Based on the Bayesian criterion, the posterior distribution of the weights is calculated by:

$$p\left(\omega\middle|t,\alpha,\sigma^2\right) = \frac{p(t|\omega,\sigma^2)p(\omega|\alpha)}{p(t|\alpha,\sigma^2)}$$
$$= (2\pi)^{-\frac{N+1}{2}}\left|\sum\right|^{-\frac{1}{2}} exp\left\{-\frac{(\omega-\mu)^T\sum^{-1}(\omega-\mu)}{2}\right\} \tag{15}$$

The posterior variance and mean of weights as follow.

$$\begin{cases} \sum = \left(\sigma^{-2}\Phi^T\Phi + A\right)^{-1} \\ \mu = \sigma^{-2}\sum\Phi^T t \end{cases} \tag{16}$$

where $A = diag(\alpha_0, \alpha_1, \cdots, \alpha_N)$

The target output likelihood distribution in Eq. (15) can be obtained by performing edge integration on the parameters.

$$p\left(t\middle|\alpha,\sigma^2\right) = \int p\left(t\middle|\omega,\sigma^2\right)p(\omega|\alpha)d\omega \tag{17}$$

According to calculation using iterative estimation method, we can get the following formula.

$$\begin{cases} \alpha_i^{new} = \dfrac{\gamma_i}{\mu_i^2} \\ \gamma_i = 1 - \alpha_i\sum_{ii} \end{cases} \tag{18}$$

μ_i is the mean of the i - th posterior weight, $\sum_{ii}$ is the i - th diagonal element of the posterior variance matrix. Use the same method to obtain noise variance.

$$\left(\sigma^2\right)^{new} = \frac{\|t-\Phi\mu\|}{N - \sum_i\gamma_i} \tag{19}$$

For a new set of inputs x_*, t_* and σ_*^2 are as below.

$$\begin{cases} t_* = \mu^T \Phi(x_*) \\ \sigma_*^2 = \sigma_{MP}^2 + \Phi(x_*)^T \sum \Phi(x_*) \end{cases} \tag{20}$$

t_* is the RVM model in the test dataset predicted output at x_*, σ_*^2 is the sum of the noise estimation variance (the first term) and the weight estimation uncertainty (the second term), σ_{MP}^2 is the variance of the noise at the end of iterations in Eq. (18) and (19).

2.3. Complementary ensemble empirical mode decomposition

Because EMD algorithm [23] exists the disadvantage of mode aliasing. To solve the problem, Torres modified EMD and named CEEMD. The algorithm can solve the EMD mode aliasing problem, overcome the low decomposition efficiency of ensemble empirical mode decomposition (EEMD) [24] and the difficulty in eliminating the noise [25]. CEEMD algorithm is as follows.

ω_i is white Gaussian noise, $i = 1,\ldots,I$, ε_i is the standard deviation of ω_i, $E_j(\cdot)$ is the j - th EMD mode, $\overline{IMF}_n(k)$ is the n - th IMF. $X(k) = x(k) + \varepsilon_0\omega_i(k)$ is new series. Apply EMD algorithm to the time series to obtain the first CEEMD IMF:

$$\overline{IMF}_1(k) = \frac{1}{I}\sum_{i=1}^{I} IMF^i(k) \tag{21}$$

For $n = 2\cdots N$, the n - th residual is $r_n(k) = r_{n-1}(k) - \overline{IMF}_n(k)$, compute the first IMF of realizations $r_n(k) + \varepsilon_k E_n(\omega_i(k))$ and get the $(n+1)$ - th CEEMD IMF by:

$$\overline{IMF}_{n+1}(k) = \frac{1}{I}\sum_{i=1}^{I} E_n[r_n(k) + \varepsilon_n E_n(\omega_i(k))] \tag{22}$$

Repeat the above procedures until the final number of extreme values of the residual is not more than two, the series can be represented as:

$$x(k) = \sum_{n=1}^{N} \overline{IMF}_n(k) + r(k) \tag{23}$$

$r(k)$ is the eventual residual.

3. Establishment and implementation of UPF-OMKRVM

In the section, the establishment and implementation of the UPF-OMKRVM method is presented in detail.

3.1. Establishment for UPF-OMKRVM

To successfully predict SOH, it is essential to build an accurate failure model. In the most system degradation models, exponential model can be widely used to characterize the process. In this paper, a dual exponential model is used to express the degradation process [26,27].

$$Q_k = a_k exp(b_k \cdot k) + c_k exp(d_k \cdot k) \tag{24}$$

Q is data, k is the size of data, and $[a_k, b_k, c_k, d_k]$ is the corresponding coefficients of the exponential model. $x_k = [a_k, b_k, c_k, d_k]$, ε_k is measurement noise, ω_k is state noise, k is cycle.

The Autoregressive (AR) model has the superiorities of simple principle, easy to use and high efficiency [28]. Hence, the AR model is adopted as the state model.

$$x_k = q + \sum_{i=1}^{p} a_j x_{k-i} + \omega_k \tag{25}$$

q is a constant term, ω_k represents independent white noise sequence, the p is order of model. We rewrite the Eq. (24) into Eq. (26):

$$\begin{aligned} Q_k &= a_k exp(b_k \cdot k) + c_k exp(d_k \cdot k) + \varepsilon_k \\ X_{k+1} &= AX_k + W_k \end{aligned} \tag{26}$$

where $X_k = [x_k, x_{k-1}, \cdots, x_{k-p+1}]^T$, $W_k = [\omega_{k+1}, 0, \cdots, 0]^T$ and $A = \begin{bmatrix} a_1 & a_2 & \cdots & a_p \\ 1 & 0 & 0 & 0 \\ 0 & 1 & 0 & 0 \\ 0 & 0 & 1 & 0 \end{bmatrix}$.

Although augmentation of the number of particles can improve the prediction precision of UPF, the prediction effect is still not ideal since the low number of effective particles, and the calculation cost will increase. Therefore, this paper focuses on how to predict the errors trend to correct the predicted value. In view of existence of noise, fluctuation and irregularity in error data, the establishment of OMKRVM model may be greatly affected. To mitigate the impact of partial volatility caused by uncertainty on UPF estimation, we reconstruct the error data by CEEMD [29].

For better predictive performance, the last known errors are combined with the OMKRVM forecasting result into consideration and the OMKRVM prediction model is established as follows:

$$e_k = g(x_{1:k}, e_{1:k-\Delta k}) + \tilde{\varepsilon}_k = \sum_{j=1}^{T-l} \Phi\omega_j + \tilde{\varepsilon}_k \tag{27}$$

where e_k is prediction errors, Φ is the kernel function matrix, T is the length of data, $\tilde{\varepsilon}$ is an independent Gaussian noise, k is cycle, Δk is steps in advance.

The kernel function in RVM plays a vital role in prediction. Mixed kernels have interpolation and extrapolation abilities, hence, we should select the multiple suitable kernels based on the characteristics of the error data instead of using a single kernel to predict the error data.

$$\begin{aligned} K_1(x_i, x_j) &= exp\left(-\|x_i - x_j\|^2 \Big/ 2\gamma^2\right) \\ K_2(x_i, x_j) &= [x_i^T \cdot x_j + 1]^d \end{aligned} \tag{28}$$

where K_1 is Gaussian kernel function, γ is kernel width, K_2 is polynomial kernel function, m is degree. The Gaussian kernel function has strong nonlinear expression ability, which can capture the local nonlinear variation trend [30,31]. The polynomial kernel function is proven to be an effective complement to the Gaussian kernel and its global generalization performance is satisfying [32]. Therefore, we select the two kernel functions to build the OMKRVM model.

$$K(x_i, x_j) = \lambda \cdot exp\left(-\|x_i - x_j\|^2 \Big/ 2\gamma^2\right) + \nu \cdot [x_i^T \cdot x_j + 1]^d \tag{29}$$

where λ and υ are the weights of kernel function, and $\lambda + \upsilon = 1$. Since the parameters of OMKRVM are difficult to directly obtain, it is feasible to determine the parameters by an optimization process. There are several methods for MKRVM parameters optimization. Zhang et.al used PSO to train MKRVM model [16], and Wang et.al used genetic algorithm (GA) optimize the parameters of MKRVM [33], and so on. Although these random search optimization algorithms are attractive, these methods are computationally intensive and the accuracy is not worth calculating [30]. In this case, only a small scale of $[\gamma, d, \lambda]$ needs to search, meta-heuristic does not work well [34]. In contrast, grid search method can achieve high accuracy with acceptable training time [35], so it is used to optimize parameters of OMKRVM model. What's more, mean square error (MSE) is used to evaluate regression performance. MSE is expressed as follows.

$$MSE = \frac{\sum_{i=1}^{N}\left[y_i - \overline{y}_i\right]^2}{N} \tag{30}$$

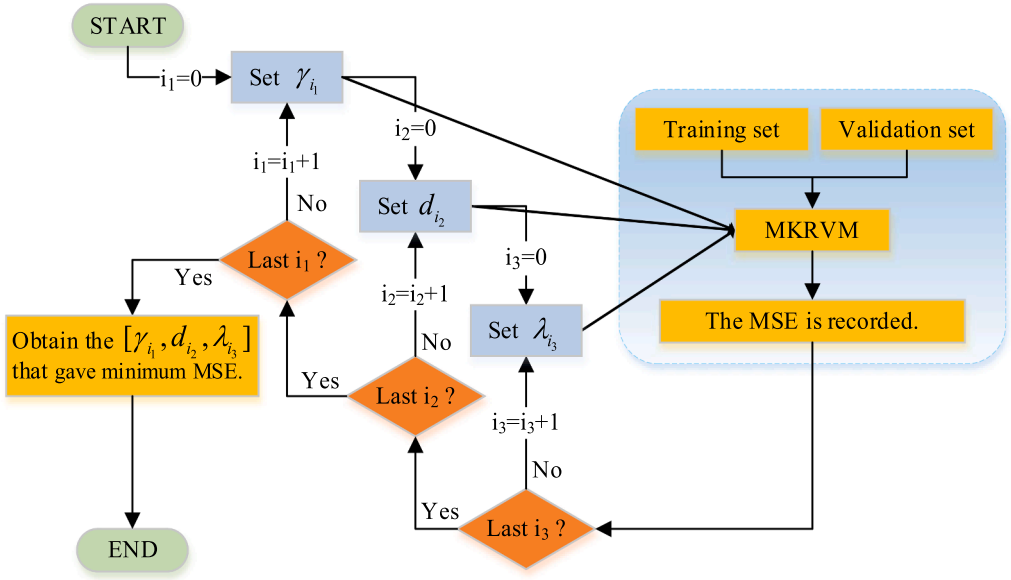

Fig. 1. Process of obtaining the optimal parameters by grid search.

where y_i is real value, $\bar{y}_i$ is predicted value, N is the size of sample. To better explain how to optimize the parameters of OMKRVM, we draw Fig. 1 for better illustration.

The training set is trained iteratively by OMKRVM to obtain the error data at the prediction point [36]. The predict values and corrected values can be recursively iterated in future time instants. After error-correction, the final results are as follows:

$$\hat{y}_k = Q_k + e_k \tag{31}$$

where k is cycle, Q_k is the predicted value by UPF, e_k is the predicted value about error data by OMKRVM, $\hat{y}_k$ is the final predicted result by UPF-OMKRVM.

The accuracy of prediction can be greatly improved by the correction at each moment, and the result shows more specific degradation characteristics.

3.2. Implementation of UPF-OMKRVM

Based on the introduction and analysis of UPF-OMKRVM, we draw a basic procedure of the UPF-OMKRVM in Fig. 2 to visualize the method.

The detail schematic diagram of UPF-OMKRVM is shown in Fig. 3. To explain the proposed method more clearly, the procedures of UPF-OMKRVM method are divided into five steps as below.

Step 1: Capacity estimation: Assume that the starting point of prognostic is T. After getting the initial parameters by training data, the capacity is estimated by UPF model based on the degradation model Eq. (26). Meanwhile, the error data are obtained.

Step 2: Error reconstruction: The residual data was reconstructed by CEEMD and the corresponding IMFs are selected by correlation coefficient to reconstruct the observation signal.

Step 3: Training OMKRVM model: The reconstructed data was used to train the OMKRVM model through Eq. (27), and the appropriate parameters of model can be obtained by grid search optimization method in Fig. 1.

Step 4: Error-correction: Predict the evolution trend of the error data by OMKRVM, and estimated value by the UPF model is corrected according Eq. (31), which is regarded as the final predicted value.

Step 5: Capacity prediction: Repeat the step 4 for the next moment, until reaching EOL. With error-correction in time, the UPF-OMKRVM is able to be well used to prediction.

3.3. Computational complexity analysis

In this paper, although the UPF-OMKRVM model obtains better prediction performance, the increase in computational complexity is also inevitable. For the UPF-OMKRVM method, the computational complexity mainly includes the following steps: (1) UPF model. (2) OMKRVM model. (3) Error-correction. (4) CEEMD method.

Since the complexity calculation is a complex work, we only consider

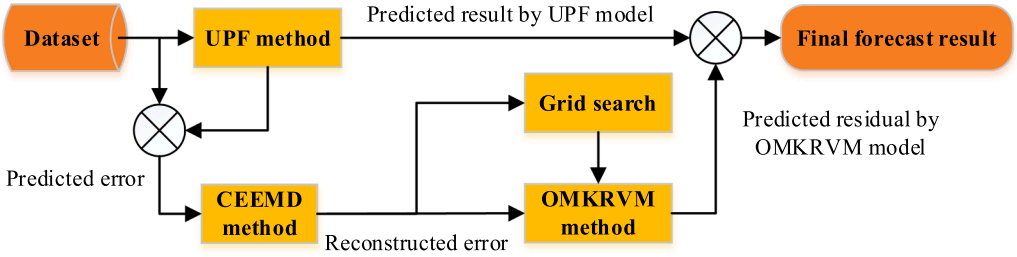

Fig. 2. The basic procedure of the UPF-OMKRVM.

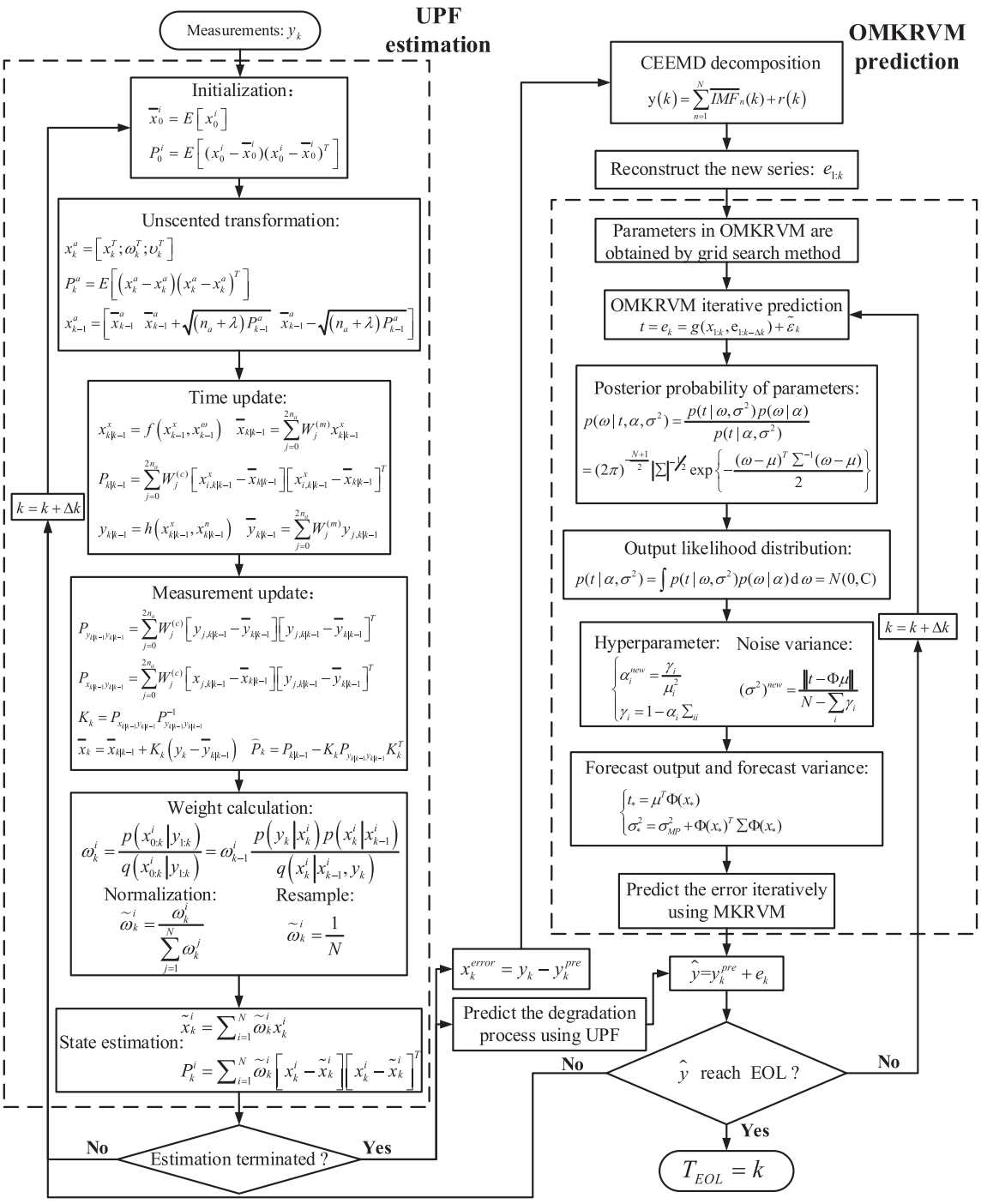

Fig. 3. Schematic diagram of the UPF-OMKRVM method.

Table 1
Comparisons of the computational complexity of UPF, OMKRVM, UPF-OMKRVM.

Method	UPF	OMKRVM	UPF-OMKRVM
Complexity	$O(4N^3 + N_o \cdot N^2)$	$O(2N^3 + 2N^2 + (41NN_l)N_eN_s)$	$O(6N^3 + (2+N_o)N^2 + (41NN_l)N_eN_s + N)$

the main calculation steps and the comparisons of the computational complexity of different methods are shown as below (see Table 1).

The size of training set is N, the number of particles is N_o, N_l refers to the number of the IMFs, N_s represents the number of siftings in EEMD, usually 100 and N_e is the ensemble number. The computational complexity of UPF method is $O(4N^3 + N_o \cdot N^2)$ [37], that of OMKRVM is $O(2N^3 + 2N^2 + (41NN_l)N_eN_s)$ [38,39] and that of UPF-OMKRVM method in this paper is $O(6N^3 + (2+N_o)N^2 + (41NN_l)N_eN_s + N)$. In summary, the computational complexity of the UPF-OMKRVM is a bit higher than that of contrast methods, but it improves the accuracy a lot.

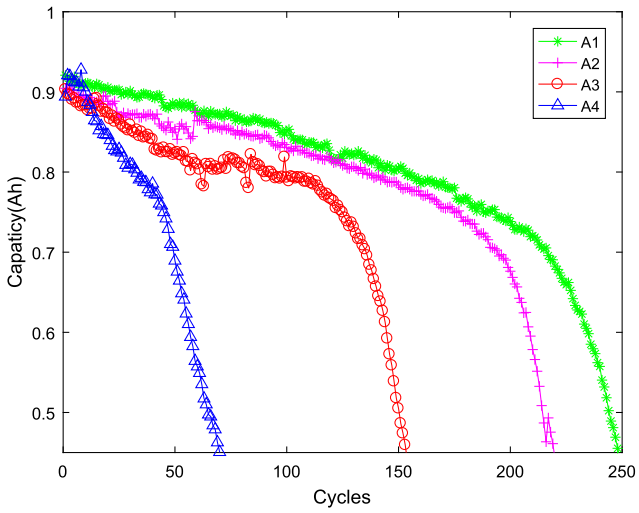

Fig. 4. CALCE lithium-ion battery capacity data.

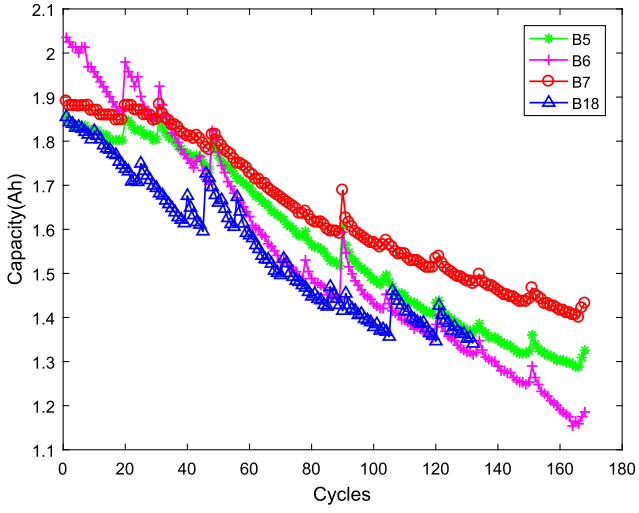

Fig. 5. NASA lithium-ion battery capacity data.

4. Experimental results and analysis

4.1. Lithium-ion battery datasets

In this paper, the experimental datasets adopt the open source lithium-ion battery capacity degradation data of the University of Maryland Center for Advanced Life Cycle Engineering (CALCE) and the Prognostics Center of Excellence (PCoE) at NASA Ames Research Center. The CALCE lithium-ion battery data was collected by Arbin BT2000 battery test system at room temperature (about 25 °C) charge and discharge tests and experimental data was collected. The rated capacity of all batteries is about 0.9 Ah. The NASA lithium-ion battery data was collected from 18650-size lithium-ion batteries. Battery charge, discharge and impedance tests were conducted on the NASA battery experimental platform at room temperature (about 25 °C). The rated capacity of the batteries is about 2 Ah. The Fig. 4 and Fig. 5 display respectively the lithium-ion battery capacity degradation data of CALCE and NASA. We find that the same battery of the same brand was tested under the same experimental conditions, but their degradation rates were different. In many studies, 80% of the rated capacity is set as the failure threshold. In this paper, the failure threshold of the A1, A2, A3, A4 is 0.72 Ah [20]. From previous research experience, failure threshold of B5, B6 and B18 are set as 1.38 Ah, as for B7, the failure threshold is set as 1.45 Ah [7,16]. The two groups of battery data are different in data length, initial value and data interference degree [19].

Table 2
Initialization of UPF model parameters.

Battery data	a	b	c	d
A1	−6.335e−10	0.1333	0.8846	−7.026e−4
A2	0.01541	−0.09874	0.8925	−2553e−4
A3	0.9058	−1.929e−3	−7.784e−3	−0.09953
A4	0.9404	−4.813e−3	−0.1055	−0.9557
B5	2.408	−4.510e−3	−0.5899	−0.02314
B6	2.092	−4.021e−3	−0.07398	−0.07210
B7	2.089	−2.942e−3	−0.2250	−0.04189
B18	0.03969	−0.09889	1.829	−2.450e−3

4.2. Parameters configuration of UPF

For the UPF algorithm, the setting of initial parameters is crucial, to make good predictions about the CALCE and NASA dataset, the exponential model is first fitted by our training data to obtain the initial parameters shown in Table 2. Moreover, the size of particles in UPF is set as 200.

Because the degradation rate of A1 and A2 battery data is lower than that of A3 and A4 battery data, and A3, A4 battery capacity has a steep decline trend in the later period, we take a ten-step-ahead prognostic for A1 and A2. Since the latter part of the sharp downward trend, a five-step-ahead prognostic for A3 and A4. As for NASA dataset, considering the large fluctuation of their capacity, the five-step-ahead prediction was also adopted. For A1, A2, A3 and A4, the prediction intervals are set as 100, 80, 60 and 35 respectively. As for B5, B6 and B7, prediction interval is set as 70, and that of B18 is 60. To decrease the effect of uncertainty on predicting RUL, we should not judge the point as the failure point once its capacity is lower than the failure threshold. In this paper, we assume that all three consecutive capacities are below the failure threshold, and then the first point is set as the failure point.

4.3. Error series reconstruction

Considering that the prediction errors by UPF has some interference, which affects the accuracy of OMKRVM prediction, we firstly adopt CEEMD method to the original error sequence. Then, IMF components (IMFs) are combined to reconstruct by correlation coefficient (between the decomposed error series and the primitive error series), the new series are synthesized. Reconstruction can effectively eliminate the noise in the signal and highlight the degraded signal characteristic.

The reconstructed series after noise reduction should not only show the long-term development tendency of the original series, but also reflect the necessary characteristics in the process of degradation. Therefore, considering the above two points, we selected the appropriate IMFs by the analysing correlation coefficient and getting rid of high frequency IMFs to reconstruct series [20]. Since the high-frequency component only shows local fluctuations and has little influence on the long-term error prediction, the first three IMFs are not selected. The correlation coefficient is lower than 0.4, which we regard as a weak correlation or even non-correlation, and the IMFs also are not selected. The correlation coefficient between 0.4 and 0.6 is considered moderate correlation, 0.6–0.8 is regard as strong correlation and the correlation

Table 3
Reconstructed error of CALCE dataset by CEEMD.

	A1		A2		A3		A4	
	Correlation coefficient	Variance ($*10^{-6}$)	Correlation coefficient	Variance ($*10^{-6}$)	Correlation coefficient	Variance ($*10^{-6}$)	Correlation coefficient	Variance ($*10^{-6}$)
IMF1	0.3946	2.5497	0.3302	5.9815	0.3228	1.3569	0.2077	6.9874
IMF2	0.3929	0.23737	0.3415	2.6639	0.3950	2.5421	0.3517	2.2366
IMF3	0.3941	0.58007	0.4756	1.6816	0.4721	3.4943	0.4524	8.0755
IMF4	0.4466	1.2889	0.5706	4.5225	0.4974	1.4820	0.6294	4.2830
IMF5	0.4411	0.61080	0.6152	2.9589	0.3663	3.8752	0.7591	2.1078
IMF6	0.4352	0.96749	0.4289	0.049840	0.7099	2.0687	–	–
IMF7	0.4402	0.80803	0.1471	0.028642	–	–	–	–
IMF8	0.4621	3.0953	–	–	–	–	–	–
original	–	15.456	–	30.125	–	64.065	–	30.381
reconstruction	**0.8678**	**9.8158**	**0.8196**	**17.291**	**0.8441**	**33.456**	**0.8567**	**20.427**

Table 4
Reconstructed error of NASA dataset by CEEMD.

	B5		B6		B7		B18	
	Correlation coefficient	Variance ($*10^{-5}$)	Correlation coefficient	Variance ($*10^{-4}$)	Correlation coefficient	Variance ($*10^{-5}$)	Correlation coefficient	Variance ($*10^{-5}$)
IMF1	0.1567	3.3313	0.0833	1.4274	0.2770	2.8746	0.0696	6.2036
IMF2	0.2554	0.99202	0.2701	0.22364	0.2456	0.94304	0.3621	6.5363
IMF3	0.3578	2.8682	0.3647	1.5258	0.2384	2.0944	0.4255	2.6651
IMF4	0.6300	2.4231	0.6499	1.2289	0.5034	1.2578	0.7455	23.264
IMF5	0.6870	2.3480	0.7215	1.1914	0.6773	2.3449	0.6819	4.9214
IMF6	0.5379	3.9645	0.5448	1.3499	0.6199	4.3410	0.1516	0.11054
IMF7	0.0293	0.63642	0.1131	0.26541	0.0640	0.53946	0.2246	0.76854
original	–	22.355	–	9.9341	–	17.975	–	60.909
reconstruction	**0.8801**	**14.618**	**0.8565**	**6.4016**	**0.8524**	**11.713**	**0.8129**	**38.148**

coefficient exceeds 0.8, which can be regarded as a extremely strong correlation. In this paper, the weak correlation IMFs are considered as low contribution to error trend, hence, these IMFs are abandoned. We only select the IMFs whose correlation coefficients exceed 0.4, which are effective for the error reconstruction. From the Table 3 and Table 4, we can clearly find that the reconstructed sequence remains strongly correlated and the variance is greatly reduced. Therefore, the reconstructed series can not only reflect the long-term tendency of residual evolution, but also reflect the high volatility of the original error data, which can be better represent the characteristics of degradation in prediction.

Original error series have more prominent peaks in respect to Fig. 6 (a), (b) and (c). Compared with the blue curve, the red curve has less noise interference. In the Fig. 6 (d), the size of data results in small error fluctuation. The error trends are similar regarding Fig. 7 (a), (b), and (c), however, the error trend regarding Fig. 7 (d) is different from that of the first three subplots due to the large fluctuation of the B18 data. The reconstructed series can better reflect the degradation trend and is not affected by noise interference regarding Fig. 6 and Fig. 7. Hence, the data after reconstruction can provide decorated input for the OMKRVM model.

4.4. Parameters optimization by grid search

For reconstruction error sequence, we use it as training set to train OMKRVM model. To make each kernel function play its predictive ability, the kernel width, the degree and the weight of each kernel function are obtained by grid search. Kernel width is γ, d represents degree, weight 1 is λ and weight 2 is ν, respectively in Eq. (29). When the kernel function contribution is almost zero to the prognostication, its weight is set to zero. The parameters of training cases are shown in Table 5. We can find that the Gaussian kernel is dominant in prediction, and the polynomial kernel is complement regarding Table 5.

4.5. Visualization of prediction results

After the establishment of OMKRVM, we can predict the capacity errors at the next moment to correct the UPF prediction value to achieve higher accuracy of prediction. To demonstrate the effectiveness of the UPF-OMKRVM, a comparative trial was conducted with the UPF and CEEMD-OMKRVM methods. The UPF method is widely used to estimate the SOH of lithium-ion batteries [12]. The CEEMD-OMKRVM method is proved to be better than the OMKRVM method in predictions of lithium-ion battery or some other datasets [16,29]. Fig. 8 and Fig. 9 shows the prognostic results of degradation process of the battery datasets by UPF, CEEMD-OMKRVM and UPF-OMKRVM methods.

The A1 and A2 lithium-ion battery datasets was predicted by ten-step-ahead of iterative prediction regarding Fig. 8 (a) and (b). Through comparing, we found that there are some irregular fluctuations in results of UPF, and CEEMD-OMKRVM performs more objectively but cannot show the details of the prediction, and it deviates in the later period. As for UPF-OMKRVM, the predicted value is significantly closer to the true value after error-correction. The predicted results of A3 and A4 by five iterative steps are given in Fig. 8 (c) and (d). Due to the large fluctuation in the middle part of the A3 data set, the red curves has a poor prediction effect in the early stage of prediction. Although the fluctuation of green curves is small in the early stage, it deviates from the real value in the later stage. Since the initial prediction value is corrected by the error evolution trend, the fluctuation of the original capacity data can be better predicted by UPF-OMKRVM method. The period of A4 data set is short, and the capacity declines sharply in the later stage of degradation, UPF and CEEMD-OMKRVM methods are hard to accurately

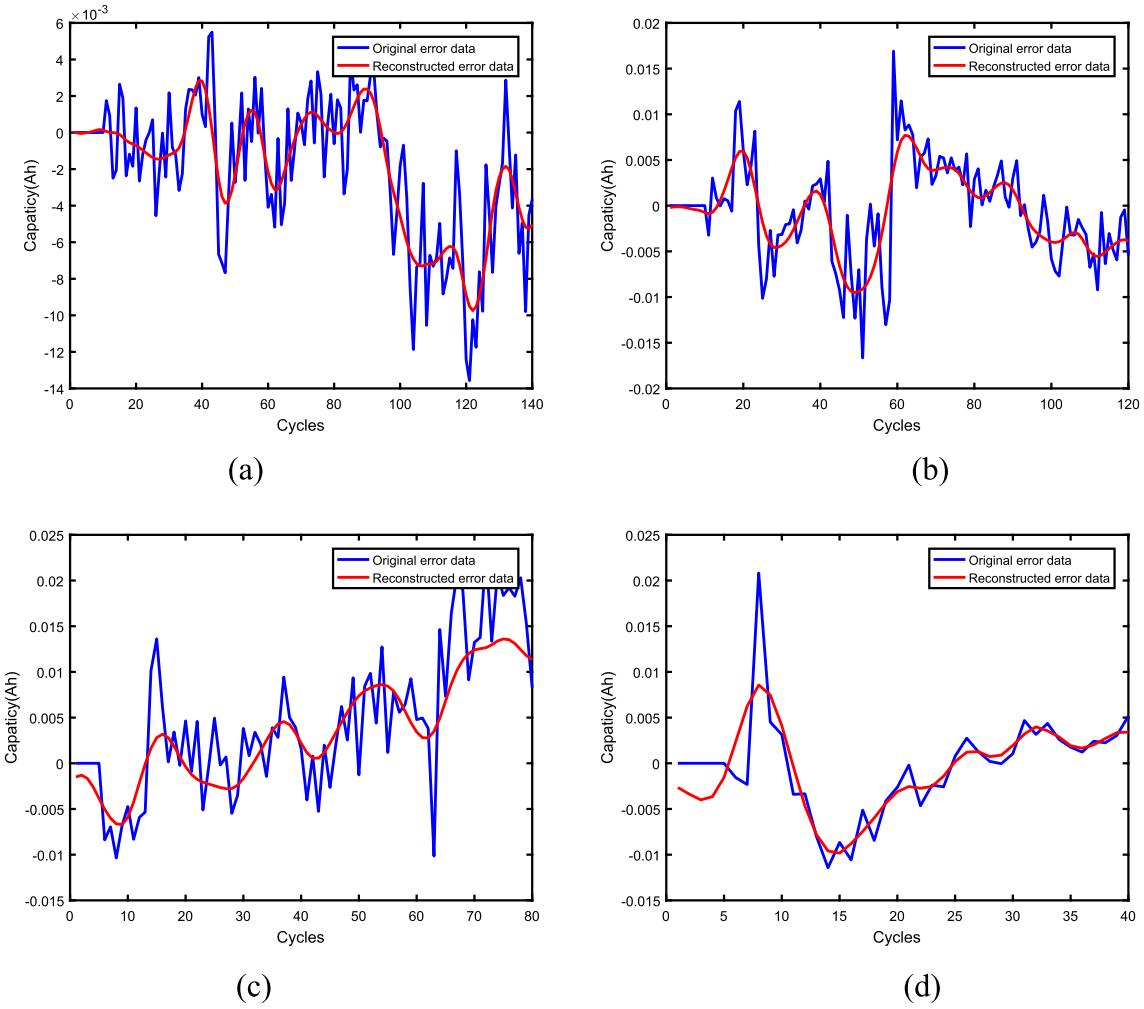

Fig. 6. Reconstruct error data and original data of CALCE (a) A1 (b) A2 (c) A3 (d) A4.

predict in time. Moreover, it is not difficult to find that UPF-OMKRVM is more robust than the other contrast methods. Therefore, the UPF-OMKRVM method outperforms the other contrast methods in CALCE lithium-ion battery RUL prediction.

For the NASA data set, we all use five-step-ahead prediction in advance. B5, B6 and B7 data sets have the same length, though the starting point and the recession rate are different, they all contain several stages of a rebound. In the Fig. 9 (a), (b) and (c), the red curves receive interference from fluctuations of data, so predicted result fluctuates. In addition, the green curves deviate original data and are difficult to show details well. The UPF-OMKRVM overcomes the shortcomings of the two methods and makes more accurate prediction results. Especially in respect to Fig. 9 (d), B18 dataset has a short period and large fluctuations. Results obtained by UPF fluctuated significantly, which are shown by the red lines. The green curve has a large deviation from the true value, and it is always above the threshold. Although the prediction effect of UPF-OMKRVM in B18 data is better than that of the other two methods, it still lags behind the performance of this method in B5, B6 and B7 (i.e., Fig. 9 (a), (b) and (c), respectively). Therefore, the hybrid method is superior to the contrast methods in NASA lithium-ion battery data.

4.6. Quantitative analysis of the prediction results

To quantitatively evaluate the precision of the prediction, we define some measurement indicators, including the accuracy indicator (AI), the root mean square error (RMSE) and the mean absolute percentage error (MAPE). The evaluation indicators are as follows:

$$AI = 1 - \frac{\left|SOH_{real}(t) - SOH_{pre}(t)\right|}{SOH_{real}(t)}$$
$$RMSE = \sqrt{\frac{1}{N}\sum_{i=1}^{N}\left(Q^{i} - \overline{Q}^{i}\right)^{2}} \tag{32}$$
$$MAPE = \frac{100\%}{N}\sum_{i=1}^{N}\left|\frac{Q - \overline{Q}^{i}}{\overline{Q}^{i}}\right|$$

where Q is the true capaticy data, $\overline{Q}$ is the predicted capaticy, SOH_{real} is the real failure point, SOH_{pre} is the predicted failure point, N is the size of prediction data. As the degradation rate of batteries is different, the prediction effect is also different. Table 6 and Table 7 show prediction steps, interval, prediction computation time and corresponding evaluation indicators.

For A1 and A2 datasets, using the 10-step-ahead prediction, the RMSE and MAPE values of UPF and CEEMD-OMKRVM methods are relatively high. As for UPF-OMKRVM, the RMSE and MAPE values obviously decline after error-correction. That is to say, the forecasting accuracy of the UPF-OMKRVM is much higher than that of the contrast methods. Since the fluctuation in the initial prediction of A3 data set, the

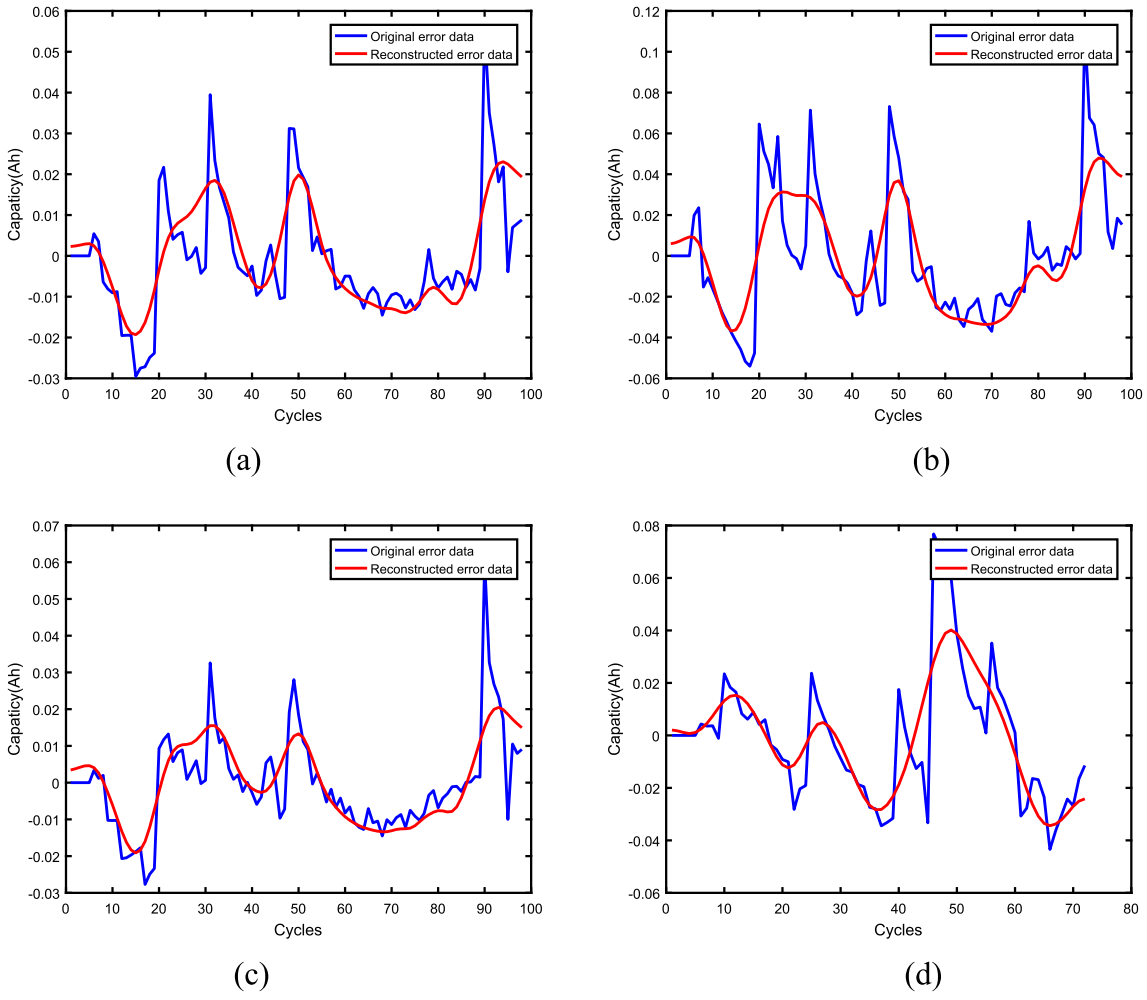

Fig. 7. Reconstruct error data and original data of NASA (a) B5 (b) B6 (c) B7 (d) B18.

prediction effect of UPF and CEEMD-OMKRVM was poor, and the RMSE and MAPE are significantly reduced after revision (i.e.,0.0046 and 0.4793). Due to the small number of data points and steep decline in the later stage of A4 dataset, UPF and CEEMD-OMKRVM could not timely predict, so the prediction effect is relatively poor. In different CALCE datasets, the UPF and CEEMD-OMKRVM methods perform differently, but both prediction effects are not as good as the UPF-OMKRVM. Among the four sets of data, AE value of the hybrid method is the highest (i.e., 0.9952, 0.9947, 1 and 0.9791), which indicates that the UPF-OMKRVM method is more effective than the other contrast methods in RUL prediction. Although the computational time of the proposed method is a bit longer than contrast methods, it improves the accuracy a lot. Moreover, the extra computing time is negligible with current computer hardware facilities.

Table 5
Kernel parameters of OMKRVM obtained by grid search.

Dataset	Kernel Width	degree	Weight 1	Weight 2
A1	3.6	1	0.721	0.279
A2	4.0	3	0.844	0.156
A3	2.7	3	0.718	0.282
A4	2.5	1	0.665	0.335
B5	6.2	–	1	0
B6	4.5	2	0.5	0.5
B7	4.2	1	0.882	0.118
B18	2.3	4	0.608	0.392

For the NASA datasets, the battery capacity rises and drops suddenly, which will affect the prediction accuracy in the degradation process. Therefore, the five-step prediction is adopted. Among the four datasets, due to the large fluctuation of data, UPF has a better prediction effect than CEEMD-MKRVM. However, on the whole, the precision of UPF prediction is unsatisfactory. Although the length of the B5, B6, B7 battery datasets is same, the starting point and degradation speed are different. The RMSE and MAPE of UPF-OMKRVM are lowest among these three methods, and AI is the highest. Whether it is to predict failure points or overall prediction accuracy, the prediction performance of the UPF-OMKRVM method is significantly superior to the other two methods. The B18 dataset is short and the fluctuation is large, the difference between the predicted failure point and the failure point actually reached 9. In contrast, the prediction results of UPF-OMKRVM are more accurate. In the process of prediction, the added time by the additional computing steps of OMKRVM can be ignored, however, the proposed method enhance the prediction accuracy markedly. Therefore, the overall prediction performance of the proposed method is better than that of the comparison algorithms.

It is easy to observe that the hybrid method outperforms UPF and CEEMD-OMKRVM with lower MAPE and RMSE values. Meanwhile, the AI values are higher compared to the other approaches. Although the

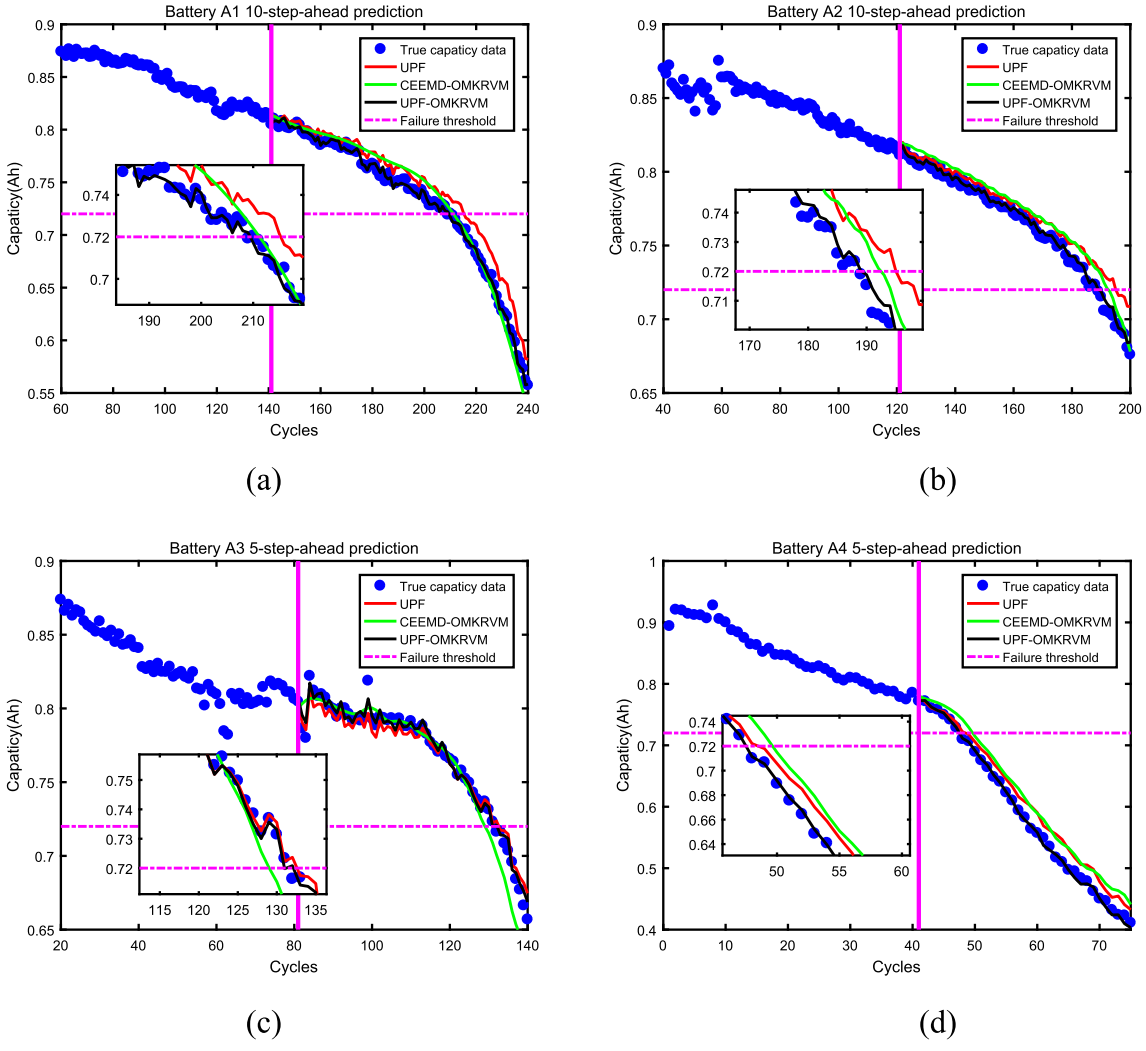

Fig. 8. The prediction results for CALCE (a) A1 (b) A2 (c) A3 (d) A4.

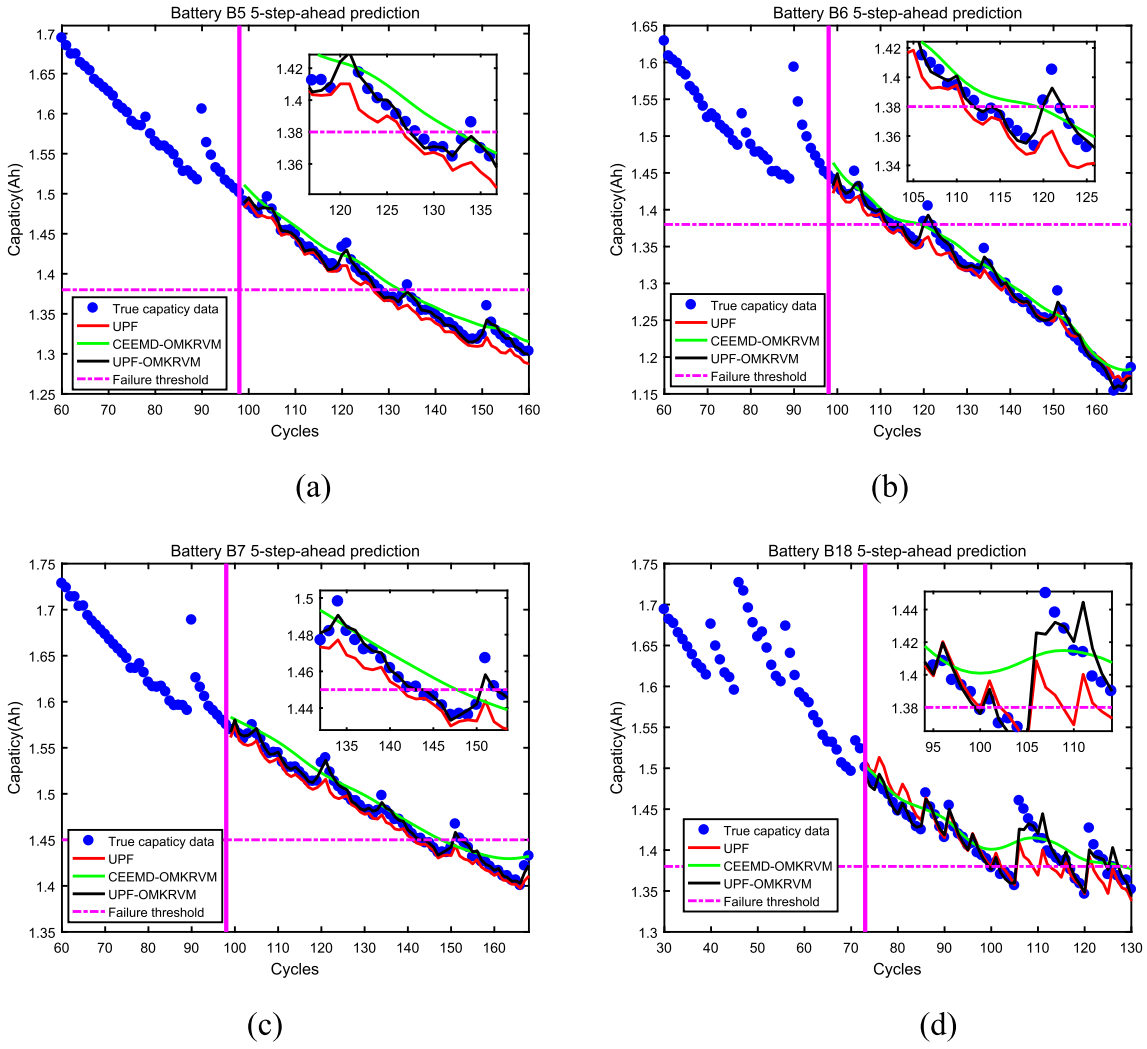

Fig. 9. The prediction results for NASA (a) B5 (b) B6 (c) B7 (d) B18.

Table 6
Prediction results for CALCE battery datasets.

Method	No	Steps	Cycle	Interval	SOH_{real}	SOH_{pre}	AI	RMSE	MAPE	Time/s
UPF	A1	10	100	[141,240]	211	217	0.9715	0.0160	1.9904	1.4058
CEEMD-OMKRVM						212	0.9952	0.0110	1.2765	0.0112
UPF-OMKRVM						**210**	**0.9952**	**0.0036**	**0.3797**	**1.4204**
UPF	A2	10	80	[121,200]	189	195	0.9682	0.0126	1.4162	1.2610
CEEMD-OMKRVM						193	0.9788	0.0089	1.0838	0.0097
UPF-OMKRVM						**190**	**0.9947**	**0.0029**	**0.2505**	**1.2931**
UPF	A3	5	60	[81,140]	132	131	0.9924	0.0075	0.7036	1.5165
CEEMD-OMKRVM						130	0.9848	0.0128	1.1548	0.0118
UPF-OMKRVM						**132**	**1**	**0.0046**	**0.4793**	**1.5303**
UPF	A4	5	35	[41,75]	48	49	0.9791	0.0226	3.7518	0.7763
CEEMD-OMKRVM						50	0.9583	0.0279	4.8970	0.0059
UPF-OMKRVM						**49**	**0.9791**	**0.0054**	**0.7591**	**0.7958**

hybrid method increases the computation time, the additional computation time is negligible under current computer hardware facilities. Moreover, for all prediction intervals, the UPF-OMKRVM is much less fluctuation than other two algorithms, which indicate that the UPF-OMKRVM method is more robust than the UPF and CEEMD-OMKRVM approaches. Even if the model-based part has larger prediction errors, the hybrid prognostic methodology can obtain more accurate results by correcting errors. Through the above contrast experiments, fully demonstrated the better accuracy, more reliable performance and more extensive applicability of the UPF-OMKRVM method.

5. Conclusion

In this paper, a new model-data hybrid prognostic methodology for the lithium-ion battery SOH and RUL estimation is proposed. After the initial estimation by UPF model and CEEMD reconstruction, the OMKRVM algorithm is used to provide prediction information for the future tendency of residual evolution. The initial estimation is corrected by the predicted tendency of residual evolution according to OMKRVM model. Since the error-correction can effectively deal with the problem of prediction deviation, the prediction performance has been

Table 7
Prediction results for NASA battery datasets.

Method	No	Steps	Cycle	Interval	SOH_{real}	SOH_{pre}	AI	RMSE	MAPE	Time/s
UPF	B5	5	70	[99,168]	129	127	0.9844	0.0143	0.8781	1.0867
CEEMD-OMKRVM						133	0.9689	0.0140	0.9733	0.0081
UPF-OMKRVM						**129**	**1**	**0.0051**	**0.2592**	**1.0992**
UPF	B6	5	70	[99,168]	113	111	0.9823	0.0134	0.7600	1.0864
CEEMD-OMKRVM						120	0.9380	0.0150	1.0010	0.0079
UPF-OMKRVM						**112**	**0.9911**	**0.0060**	**0.3519**	**1.0963**
UPF	B7	5	70	[99,168]	144	142	0.9861	0.0107	0.5994	1.1251
CEEMD-OMKRVM						148	0.9722	0.0131	0.7904	0.0087
UPF-OMKRVM						**145**	**0.9930**	**0.0041**	**0.1953**	**1.1401**
UPF	B18	5	60	[73,132]	102	101	0.9901	0.0205	1.0269	0.9491
CEEMD-OMKRVM						128	0.7450	0.0211	1.2142	0.0068
UPF-OMKRVM						**103**	**0.9901**	**0.0109**	**0.5344**	**0.9564**

significantly improved. Compared with related UPF and CEEMD-OMKRVM methods, the prediction results of UPF-OMKRVM has higher accuracy, the smaller fluctuation and more robust. Therefore, we conclude that the proposed method performs well in lithium-ion battery SOH and RUL prediction.

The current work indicates the hybrid method has practical significance in the prediction of RUL. But the use of multiple algorithms can lead to increase the computational costs, especially when the dataset is relatively large. In future work, we may take the optimization algorithms as the main research object and explore a more practical approach for constructing error data.

CRediT authorship contribution statement

Xiaofei Sun: Conceptualization, Methodology, Software, Writing - original draft, Writing - review & editing. **Kai Zhong:** Methodology, Formal analysis, Writing - review & editing. **Min Han:** Conceptualization, Supervision, Project administration, Funding acquisition.

Declaration of Competing Interest

The authors declare that they have no known competing financial interests or personal relationships that could have appeared to influence the work reported in this paper.

Acknowledgment

This work is supported by the National Key Research and Development Program of China (2016YFC0400903) and the Fundamental Research Funds for the Central Universities (DUT20LAB114, DUT2018TB06).

References

[1] M. Kordestani, M. Saif, M.E. Orchard, et al., Failure Prognosis and applications—a survey of recent literature, IEEE Trans. Reliab. (2019).
[2] S. Yin, S.X. Ding, D. Zhou, Diagnosis and prognosis for complicated industrial systems—Part II, IEEE Trans. Ind. Electron. 63 (5) (2016) 3201–3204.
[3] K. Zhong, M. Han, T. Qiu, et al., Distributed dynamic process monitoring based on minimal redundancy maximal relevance variable selection and bayesian inference, IEEE Trans. Control Syst. Technol. (2019).
[4] D. Liu, J. Zhou, D. Pan, et al., Lithium-ion battery remaining useful life estimation with an optimized Relevance Vector Machine algorithm with incremental learning, Measurement 63 (2015) 143–151.
[5] Z. Liu, Z. Jia, C.M. Vong, et al., A patent analysis of prognostics and health management (PHM) innovations for electrical systems, IEEE Access 6 (2018) 18088–18107.
[6] K. Zhong, M. Han, B. Han, Data-driven based fault prognosis for industrial systems: a concise overview, IEEE/CAA J. Autom. Sin. (2019).
[7] Q. Qin, S. Zhao, S. Chen, et al., Adaptive and robust prediction for the remaining useful life of electrolytic capacitors, Microelectron. Reliab. 87 (2018) 64–74.
[8] H. Wang, W. Song, E. Zio, et al., Remaining useful life prediction for lithium-ion batteries using fractional Brownian motion and fruit-fly optimization algorithm, Measurement 107904 (2020).
[9] J. Guo, Z. Li, M. Li, A review on prognostics methods for engineering systems, IEEE Trans. Reliab. (2019).
[10] C.K.R. Lim, D. Mba, Switching Kalman filter for failure prognostic, Mech. Syst. Sig. Process. 52 (2015) 426–435.
[11] H. Zhang, Q. Miao, X. Zhang, et al., An improved unscented particle filter approach for lithium-ion battery remaining useful life prediction, Microelectron. Reliab. 81 (2018) 288–298.
[12] D. Liu, X. Yin, Y. Song, et al., An on-line state of health estimation of lithium-ion battery using unscented particle filter, IEEE Access 6 (2018) 40990–41001.
[13] X. Wang, B. Jiang, N. Lu, et al., Dynamic fault prognosis for multivariate degradation process, Neurocomputing 275 (2018) 1112–1120.
[14] C. Zhang, Y. He, S. Jiang, et al., Analog circuit fault prognostic approach using optimized RVM, Int. J. Perform. Eng. 15 (5) (2019).
[15] X. Wang, B. Jiang, N. Lu, Adaptive relevant vector machine based RUL prediction under uncertain conditions, ISA Trans. 87 (2019) 217–224.
[16] C. Zhang, Y. He, L. Yuan, S. Xiang, Capacity prognostics of lithium-ion batteries using EMD denoising and multiple kernel RVM, IEEE Access 5 (2017) 12061–12070.
[17] S. Yuchen, L.I.U. Datong, H.O.U. Yandong, et al., Satellite lithium-ion battery remaining useful life estimation with an iterative updated RVM fused with the KF algorithm, Chin. J. Aeronaut. 31 (1) (2018) 31–40.
[18] X. Zheng, H. Fang, An integrated unscented kalman filter and relevance vector regression approach for lithium-ion battery remaining useful life and short-term capacity prediction, Reliab. Eng. Syst. Saf. 144 (DEC.) (2015) 74–82.
[19] Y. Chang, H. Fang, A hybrid prognostic method for system degradation based on particle filter and relevance vector machine, Reliab. Eng. Syst. Saf. 186 (JUN.) (2019) 51–63.
[20] Y. Chang, H. Fang, Y. Zhang, A new hybrid method for the prediction of the remaining useful life of a lithium-ion battery, Appl. Energy 206 (nov.15) (2017) 1564–1578.
[21] W. Wei, S. Gao, Y. Zhong, et al., Adaptive square-root unscented particle filtering algorithm for dynamic navigation, Sensors 18 (7) (2018) 2337.
[22] D. Kong, Y. Chen, N. Li, et al., Relevance vector machine for tool wear prediction, Mech. Syst. Sig. Process. 127 (2019) 573–594.
[23] N.E. Huang, Z. Shen, S.R. Long, et al., The empirical mode decomposition and the Hilbert spectrum for nonlinear and non-stationary time series analysis, Proc. Roy. Soc. London Ser. A: Math. Phys. Eng. Sci. 1998 (454) (1971) 903–995.
[24] Z. Wu, N.E. Huang, Ensemble empirical mode decomposition: a noise-assisted data analysis method, Adv. Adaptive Data Anal. 1 (01) (2009) 1–41.
[25] M.E. Torres, M.A. Colominas, G. Schlotthauer, et al., A complete ensemble empirical mode decomposition with adaptive noise, in: 2011 IEEE international conference on acoustics, speech and signal processing (ICASSP), IEEE, 2011, pp. 4144–4147.
[26] F. Yang, D. Wang, Y. Xing, et al., Prognostics of Li (NiMnCo) O2-based lithium-ion batteries using a novel battery degradation model, Microelectron. Reliab. 70 (2017) 70–78.
[27] W. He, N. Williard, M. Osterman, et al., Prognostics of lithium-ion batteries based on Dempster-Shafer theory and the Bayesian Monte Carlo method, J. Power Sources 196 (23) (2011) 10314–10321.
[28] H. Akaike, A new look at the statistical model identification, IEEE Trans. Autom. Control 19 (6) (1975) 716–723.
[29] Y. Xu, M. Zhang, Q. Zhu, et al., An improved multi-kernel RVM integrated with CEEMD for high-quality intervals prediction construction and its intelligent modeling application, Chemomet. Intell. Lab. Syst. 171 (2017) 151–160.
[30] X. Zhu, Z. Huang, H.T. Shen, et al., Dimensionality reduction by Mixed Kernel Canonical Correlation Analysis, Pattern Recogn. 45 (8) (2012) 3003–3016.
[31] K. Zhong, M. Han, T. Qiu, et al., Fault diagnosis of complex processes using sparse kernel local Fisher discriminant analysis, IEEE Trans. Neural Networks Learn. Syst. 31 (5) (2019) 1581–1591.
[32] H. Yang, Z. Xu, J. Ye, et al., Efficient sparse generalized multiple kernel learning, IEEE Trans. Neural Networks 22 (3) (2011) 433–446.
[33] F. Wang, K. Gan, C. Wu, et al., Comparative study on gesture recognition using multiple kernel learning via multi-mode information fusion. 2017 IEEE 7th Annual International Conference on CYBER Technology in Automation, Control, and Intelligent Systems (CYBER), IEEE, 2017.
[34] J.M. Bernal-de-Lázaro, O. Llanes-Santiago, A. Prieto-Moreno, et al., Enhanced dynamic approach to improve the detection of small-magnitude faults, Chem. Eng. Sci. (2016). S0009250916300926.

[35] K.E.S. Pilario, Y. Cao, M. Shafiee, Mixed kernel canonical variate dissimilarity analysis for incipient fault monitoring in nonlinear dynamic processes, Comput. Chem. Eng. (2018).
[36] F. Chen, Y. Yang, B. Tang, et al., Performance degradation prediction of mechanical equipment based on optimized multi-kernel relevant vector machine and fuzzy information granulation, Measurement (2020).
[37] A. Minetto, G. Falco, F. Dovis, On the trade-off between computational complexity and collaborative GNSS hybridization, in: 2019 IEEE 90th Vehicular Technology Conference (VTC2019-Fall), IEEE, 2019, pp. 1–5.
[38] C. Silva, B. Ribeiro, Scaling text classification with relevance vector machines, in: 2006 IEEE international conference on systems, man and cybernetics, vol. 5, IEEE, 2006, pp. 4186–4191.
[39] Y.H. Wang, C.H. Yeh, H.W.V. Young, et al., On the computational complexity of the empirical mode decomposition algorithm, Physica A 400 (2014) 159–167.